Formulation and Characterization of Power System Electromechanical Oscillations

Bin Wang, *Student Member, IEEE*, Kai Sun, *Senior Member, IEEE*

***Abstract*—When generators of a power system are subject to a large disturbance, their electromechanical oscillations (EOs) are essentially nonlinear as observed from their rotor angle waveforms due to the nonlinear power network. However, traditional modal analysis has not given enough considerations to nonlinearities in EOs. This paper analytically formulates the accurate oscillation frequency (OF) of an EO mode addressing nonlinearities. It is revealed that when the system model and condition are fixed, the OF of any EO mode is energy-dependent as a function of the oscillation amplitude (OA). That is characterized by a new tool named Frequency-Amplitude (F-A) curve regarding each mode, from which the frequency decreases from the natural frequency toward zero when the amplitude grows to a critical threshold. The paper proves that an F-A curve is actually a projection of the system trajectory between the stable equilibrium and the stability boundary onto the OF-OA plane regarding one mode. Based on the concept of F-A curve, a stability index is defined and estimated from measurements for online angle stability analysis. The proposed methodology is presented in detail using a SMIB system and then demonstrated on the IEEE 9-bus system and WECC 179-bus system having multiple EO modes.**

***Index Terms*—Electromechanical oscillation, F-A curve, frequency-amplitude curve, nonlinear oscillation, oscillation frequency, phasor measurement unit, PMU, rotor angle stability.**

I. Introduction

INTER-AREA oscillations have been threatening system operations and stability since the beginning of interconnecting power systems over weak tie lines in the 1960s [1]. An interconnected power system is essentially a nonlinear oscillator network, so its electromechanical oscillations (EOs) have inherent nonlinearities and are different from oscillations with a linear system. Both model-based and measurement-based have been proposed for analyzing EOs in the past several decades [2]-[5]. However, most of the methods do not take the nonlinearities with a power system into account and only use a linearized system model to study EOs from a small-signal stability point of view. A few methods address the nonlinearities with an EO mode either to limited orders based on a pre-assumed normal form or from a purely signal-processing perspective lacking insights into the nonlinear nature of the EO mode.

Current model-based methods in the literature include the eigenanalysis on the linearized system model and normal form methods on a truncated Taylor expansion of the system. The eigenanalysis analyzes the system behavior at a certain operating point and defines the frequency, damping, mode shape, participation factor and some other concepts based on the eigenvalues and eigenvectors of the associated linearized system for benchmarking other linear modal analyses. Normal form based methods usually extend the linearized system model to a polynomial form that models nonlinearities of the system up to a certain order, such as the 2nd order in [6] and 3rd order in [7]. Thus, the definitions of frequency and damping are extended and the concept of nonlinear modal interaction is introduced.

Measurement-based methods include two categories: 1) linear methods, such as the Prony method [8], Eigensystem Realization Algorithm [9] and Matrix Pencil method [10], always assume an EO to be harmonic with its constant frequency, damping and phasing during a specific time period, which works accurately for a small EO but contains non-negligible errors for an EO of large amplitude; 2) nonlinear methods, such as Hilbert-Huang Transformation [11] and Energy Tracking Operators based method [12], are purely based on signal processing and may not be insightful to understand the nonlinear nature with an EO mode. For instance, if the frequency of one EO mode fluctuates during the window of measurements, a signal processing based method may tell two or more separate modes [13].

Based on our previous studies, an EO model in fact drifts its frequency all over the swings [13], which can be captured by a phase-locked loop based method applied to the measurements [14]. An approximate analytic approach based on differential Groebner basis and harmonic balance constructs an approximate expression for the oscillation frequency on a single-machine infinite-bus (SMIB) system considering certain nonlinearities [15]. There is yet a lack of analytical studies addressing the nonlinear mechanism of an EO mode.

This paper presents both model-based and measurement-based approaches to study nonlinearities of power system EOs due to the networking of generator swing equations. First, the oscillation frequency of an undamped SMIB system is analytically formulated to discover the frequency-energy dependency with an EO mode under disturbances around a given stable

This work was supported in part by NSF CAREER Award (ECCS-1553863) and in part by in part by the ERC Program of the NSF and DOE under Grant EEC-1041877.

B. Wang and K. Sun are with the University of Tennessee, Knoxville, TN, 37996 USA. (e-mail: bwang13@vols.utk.edu, kaisun@utk.edu).

equilibrium point (SEP) of the system. Accordingly, a new tool named frequency-amplitude (F-A) curve is proposed to characterize EOs regarding a specific mode. A measurement-based method is proposed to estimate the F-A curve and an associated angular stability margin index. The impacts from the modeling of more details and excitation systems of generators are also investigated.

The remainder of this paper is organized as follows. Section II discusses nonlinearities of an EO mode. Section III presents an analytical formulation on the frequency of one specific mode using a SMIB system and associated approximate calculation. Section IV introduces the concept of the F-A curve and its application in angle stability analysis. Section V proposes a measurement-based method for estimating the F-A curve, which is then validated on multiple EO modes of the IEEE 9-bus system and WECC 179-bus system in Section VI with the effects of the details of generator models and excitation systems investigated. Conclusion is provided at the end.

II. Nonlinearities with Power System Electromechanical Oscillations

This section discusses two nonlinearity-induced characteristics of the EO of a SMIB power system.

A. Natural frequency of a SMIB system

Consider the swing equation of the SMIB power system in the classical model as shown in Fig.1, where $\delta = \Delta\delta + \delta_s$.

$$\Delta\ddot{\delta} = \frac{\omega_0}{2H}\left(P_m - P_e\right) - \frac{D}{2H}\Delta\dot{\delta} \tag{1}$$

$$\begin{cases} P_m = P_{max}\sin\delta_s \\ P_e = P_{max}\sin\left(\Delta\delta + \delta_s\right) \end{cases} \tag{2}$$

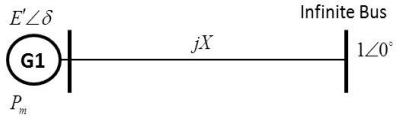

Fig.1. An SMIB power system

$\Delta\delta$ is the relative rotor angle to its steady state δ_s; ω_0 is the synchronous frequency; E', P_m and P_e represent the per-unit field voltage, mechanic power and electric power, respectively; H and D represent the inertia and damping constants of the machine, respectively. For simplicity, P_m, E' and all parameters are assumed to remain the same before and after the disturbance; $P_{max}=E'\cdot 1/X$ is the maximum transfer power.

An accurate closed-form solution of (1) does not exist. Its numerical solution can be obtained by solving an initial value problem of the differential equation. For example, consider parameters H=3s, D=0, X=1 p.u., E'=1.7 p.u., δ_s=15° and $\omega_0=2\pi\times 60$ rad/s. Then, P_{max} and P_m are calculated to be 1.7 p.u. and 0.44 p.u., respectively. There are two equilibrium points: the SEP at δ_s=15° and the UEP (unstable equilibrium point) at δ_{uep}=180°−15°=165°. The natural frequency of the only EO mode is 1.62Hz from (3), where β denotes $P_{max}\omega_0/2H$ for simplicity.

$$f_n = \sqrt{\beta\cos\delta_s}\,/2\pi = \sqrt{\frac{P_{max}\omega_0}{2H}\cos\delta_s}\,/2\pi \tag{3}$$

The nonlinearity inherit to (2) is mainly because of P_e as a sine function of $\Delta\delta$. Similarly, for a multi-machine system, the networking of swing equations makes the electric power of any machine be a nonlinear sine function of all rotor angles.

B. Nonlinearities of an EO mode

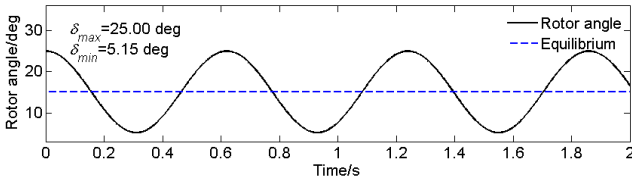

Fig.2. Rotor angle in scenario 1

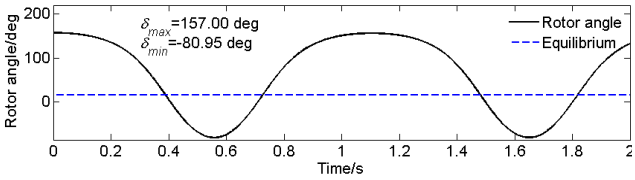

Fig.3. Rotor angle in scenario 2

Let $\delta_0=\delta(0)$ and $\dot{\delta}_0=\dot{\delta}(0)$ as the initial states. Consider two scenarios shown in Fig.2 and Fig.3, which are numerical solutions of (1) with different initial states: Scenario 1 with δ_0=25° and $\dot{\delta}_0=0$ has nearly linear swings after a small disturbance; Scenario 2 with δ_0=157° and $\dot{\delta}_0=0$ has significantly nonlinear swings after a large disturbance. There are two observations from Fig.2 and Fig.3 about nonlinearities in an EO:

1) Asymmetry

First, the waveform and amplitudes of the oscillation are not symmetric about the SEP. In Fig.2, the positive and negative amplitudes of the rotor angle are 10° and 9.85°, respectively, which are fairly close but still different; in Fig.3, the difference is as large as 46°. Second, the two halves of one cycle of the oscillation are not symmetric, either. In Fig.3, the time length of any upper half of cycle is about 0.76s while the length of any lower half is only about 0.33s. Comparison of Fig.2 and Fig.3 indicates that the system exhibits more significant asymmetry in both the amplitude and period with a larger oscillation.

2) Frequency-Amplitude dependency

Due to the above asymmetry, an oscillation curve is not harmonics and cannot be represented by any sinusoidal signal having a constant frequency. In addition, the term "oscillation amplitude" becomes ambiguous because the positive amplitude is different from the negative one.

For simplicity, the following definitions for the oscillation frequency and amplitude will be used for introducing the second nonlinear characteristic of an EO mode:

- Oscillation frequency (OF): the reciprocal of the time period associated with any full cycle of the oscillation.
- Oscillation amplitude (OA): the largest deviation from the equilibrium point of the oscillation.

With the above definitions, we have OF=1.61Hz and OA=10^0 for scenario 1 and OF=0.92Hz and OA=142° for scenario 2. It can be concluded that the OF decreases with OA. Such a phenomenon is also observed in [16]. By testing more

scenarios, the relation between OF and OA at a higher resolution is shown in Table I.

TABLE I. RELATION BETWEEN OF AND OA IN A SMIB SYSTEM

OA/deg	OF/Hz	OA/deg	OF/Hz	OA/deg	OF/Hz
10	**1.61**	90	1.37	130	1.07
30	1.59	100	1.31	136	1.00
50	1.54	110	1.24	**142**	**0.92**
70	1.46	120	1.16	145	0.83

C. Shortcomings with the harmonic oscillation assumption

Traditional power system modal analysis tools assume harmonic oscillations so as to decompose an EO as a sum of positively or negatively damped sinusoids. The above two nonlinear characteristics indicate that a power system EO cannot be treated as a harmonic oscillation.

In the following, to illustrate that why the harmonic oscillation assumption is inaccurate, the Matrix Pencil analysis [10] is used. The rotor angles in the above two scenarios can be decomposed into multiple harmonic components with different frequencies and amplitudes as shown in Table II. The Matrix Pencil analysis may quantify the nonlinearities with an EO mode from the perspective of harmonics but it is unable to accurately exhibit the aforementioned two nonlinear characteristics: 1) the asymmetry in the OA cannot be seen directly from the results because each decomposed periodic component is harmonic, i.e. a symmetric sinusoid; 2) when obvious nonlinearities show up in Scenario 2, the estimated OF, i.e. 1.09Hz, is far away from the more accurate 0.92Hz in Table I. Similarly, many other analyses based on the harmonic oscillation assumption cannot properly discover those two characteristics, either.

TABLE II. MATRIX PENCIL ANALYSIS ON THE TWO TESTED SCENARIOS

Scenario	Component	Frequency/Hz	Amplitude/deg
1	1	0	15.12
	2	**1.61**	**9.93**
	3	3.22	0.04
2	1	0	73.52
	2	**1.09**	**110.56**
	3	2.14	25.30
	4	4.42	1.06

To accurately characterize EOs, the above definitions of OF and OA are adopted in the rest of the paper as generalizations of their traditional definitions with linear systems.

III. FORMULATION OF THE OF FOR A SMIB POWER SYSTEM

This section formulates the OF for an SMIB power system without damping. Later in Section VI, the effects of damping will be investigated.

A. Formulation of the OF

Due to the asymmetry with an EO curve, the motions in the upper and lower halves of each cycle are different and hence should be formulated separately. Assume that the positive and negative extreme points (i.e. the peak and valley) of δ are known, respectively denoted by $\delta_{\max}$ and $\delta_{\min}$. The upper half of cycle T_u is the time taken for δ to increase from SEP δ_s to $\delta_{\max}$ plus the time to return. According to the symmetry of the upper half of cycle, only the upswing is considered.

Any position δ in one upswing can be linked to peak $\delta_{\max}$ by the law of conservation of energy. Define the potential energy at the SEP to be zero. The kinetic and potential energies of the system at any $\Delta\delta$ within the upswing are determined by

$$\begin{cases} E_k = \dfrac{H}{\omega_0}\left(\dfrac{d\Delta\delta}{dt}\right)^2 \\ E_p = P_{max}\left(\cos\delta_s - \cos(\Delta\delta+\delta_s) - \Delta\delta\sin\delta_s\right) \end{cases} \tag{4}$$

Note that during the upswing $d\Delta\delta/dt>0$. Solve dt in (4) as

$$dt = \frac{1}{\sqrt{2\beta}}\frac{d\Delta\delta}{\sqrt{\cos(\Delta\delta+\delta_s)-\cos\delta_{\max}+(\Delta\delta+\delta_s-\delta_{\max})\sin\delta_s}} \tag{5}$$

Integrate its both sides about one upswing to obtain the total time for $\Delta\delta$ to increase from 0 to $\delta_{\max}-\delta_s$, doubling which gives the upper half of cycle T_u

$$T_u(\delta_{\max}) = \sqrt{\frac{2}{\beta}}\int_0^{\delta_{\max}-\delta_s}\frac{d\Delta\delta}{\sqrt{\cos(\Delta\delta+\delta_s)-\cos\delta_{\max}+(\Delta\delta+\delta_s-\delta_{\max})\sin\delta_s}} \tag{6}$$

Similarly, the lower half of cycle T_r will be

$$T_r(\delta_{\min}) = \sqrt{\frac{2}{\beta}}\int_{\delta_{\min}-\delta_s}^{0}\frac{d\Delta\delta}{\sqrt{\cos(\Delta\delta+\delta_s)-\cos\delta_{\min}+(\Delta\delta+\delta_s-\delta_{\min})\sin\delta_s}} \tag{7}$$

Then, define the OF f as (8)

$$f(\delta_{\max},\delta_{\min}) = \frac{1}{T_u+T_r} \tag{8}$$

The above formulation of OF is directly from the nonlinear swing equation of the SMIB system based on the law of conservation of energy, which contains two elliptic integrals of the first kind, i.e. (6) and (7). It can be seen that the OF is a function of $\delta_{\max}$ and $\delta_{\min}$ when the SEP and all other parameters are fixed. Also note that both $\delta_{\max}$ and $\delta_{\min}$ depend on the total energy of the system while only one of them is independent, which means that given one, the other one is uniquely determined.

B. Determination of $\delta_{\max}$ and $\delta_{\min}$

One method is to determine $\delta_{\max}$ and $\delta_{\min}$ from the system model with initial values δ_0 and $\dot{\delta}_0$ given: because the kinetic energy is zero when the system reaches an extreme point δ_{ep}, either $\delta_{\max}$ or $\delta_{\min}$, from the conservation of energy law, there is equation (9) about δ_{ep}; the positive and negative roots closest to the SEP are respectively $\delta_{\max}$ and $\delta_{\min}$.

$$\dot{\delta}_0^2 + \beta[\cos\delta_{ep} - \cos\delta_0 + (\delta_{ep}-\delta_0)\sin\delta_s] = 0 \tag{9}$$

An alternative method is to estimate $\delta_{\max}$ and $\delta_{\min}$ directly from measurement data: if the time series of δ is measured, $\delta_{\max}$ and $\delta_{\min}$ can be estimated from the maximum and minimum from the measurements.

C. Calculation of the OF

To calculate the OF in (8), two integrals in (6) and (7) need to be calculated by either numerical or analytical methods. In the following, a power series based analytical approach is proposed to give an approximate estimate of the OF. Due to the similarity of two integrals, only calculation of (6) is presented in detail. The basic idea of the power series based approach is to expand the integrand of (6) by a power series and find a proper transformation to make each term integrable. The first step is the coordinate transformation by (10), which ensures the

integrability of each term in the expansion.

$$\sin\phi = \sin\frac{\Delta\delta}{2}\Big/\sin\left(\frac{\delta_{\max}-\delta_s}{2}\right) \tag{10}$$

Denote k=sin(($\delta_{\max}-\delta_s$)/2) for simplicity and we have

$$\begin{cases}\Delta\delta = 2\arcsin(k\sin\phi)\\ d\Delta\delta = \dfrac{2k\cos\phi}{\sqrt{1-k^2\sin^2\phi}}d\phi\end{cases} \tag{11}$$

Note that when $\Delta\delta$ increases from 0 to $\delta_{\max}-\delta_s$ during the up-swing, ϕ increases from 0 to $\pi/2$. Then, equation (6) becomes

$$T_u = \int_0^{\pi/2} h_u(\sin\phi)d\phi = \int_0^{\pi/2}\sqrt{\frac{2}{\beta}}\cdot\frac{2k\cos\phi}{\sqrt{1-k^2\sin^2\phi}}\left[p_u(\sin\phi)\right]^{\frac{1}{2}}d\phi \tag{12}$$

$$h_u(x) = \sqrt{\frac{2}{\beta}}\cdot\frac{2k\sqrt{1-x^2}}{\sqrt{1-(kx)^2}}\cdot\left[p_u(x)\right]^{-\frac{1}{2}} \tag{13}$$

$$\begin{aligned}p_u(x) = {}&\cos\left(\delta_s + 2\arcsin(kx)\right) - \cos(\delta_s + 2\arcsin k)\\ &+\left(2\arcsin(kx) - 2\arcsin k\right)\sin\delta_s\end{aligned} \tag{14}$$

Expand $h_u(x)$ at x=0 as (15) and substitute it into (12) with x=sinϕ to obtain (16).

$$h_u(x) = \sum_{i=0}^{\infty}\frac{h_u^{(i)}(0)}{i!}x^i \tag{15}$$

$$T_u = \int_0^{\pi/2}\left(\sum_{i=0}^{\infty}\frac{h_u^{(i)}(0)}{i!}\sin^i\phi\right)d\phi = \sum_{i=0}^{\infty}\left(\frac{h_u^{(i)}(0)}{i!}\int_0^{\pi/2}\sin^i\phi d\phi\right) \tag{16}$$

Using formula (17), express T_u by the sum of a series in (18)

$$\int_0^{\pi/2}\sin^i\varphi d\varphi = \begin{cases}\dfrac{(i-1)!!}{i!!}\cdot\dfrac{\pi}{2}, \text{ for } i = 0,2,4,\cdots\\ \dfrac{(i-1)!!}{i!!}, \text{ for } i = 1,3,5,\cdots\end{cases} \tag{17}$$

$$T_u = \sum_{i=0}^{\infty}t_{u,i} = \sum_{j=0}^{\infty}\left(t_{u,2j} + t_{u,2j+1}\right) \tag{18}$$

$$t_{u,2j} = \frac{h_u^{(2j)}(0)}{\left((2j)!!\right)^2}\cdot\frac{\pi}{2}\ ,\ \ t_{u,2j+1} = \frac{h_u^{(2j+1)}(0)}{\left((2j+1)!!\right)^2} \tag{19}$$

Similarly, T_r can be calculated by (20)-(23).

$$T_r = \sum_{i=0}^{\infty}t_{r,i} = \sum_{j=0}^{\infty}\left(t_{r,2j} + t_{r,2j+1}\right) \tag{20}$$

$$t_{r,2j} = \frac{h_r^{(2j)}(0)}{\left((2j)!!\right)^2}\cdot\frac{\pi}{2}\ ,\ \ t_{r,2j+1} = \frac{h_r^{(2j+1)}(0)}{\left((2j+1)!!\right)^2} \tag{21}$$

$$h_r(x) = \sqrt{\frac{2}{\beta}}\cdot\frac{2k'\sqrt{1-x^2}}{\sqrt{1-(k'x)^2}}\cdot\left[p_r(x)\right]^{-\frac{1}{2}} \tag{22}$$

$$\begin{aligned}p_r(x) = {}&\cos\left(\delta_s + 2\arcsin(k'x)\right) - \cos(\delta_s - 2\arcsin k')\\ &+\left(2\arcsin(k'x) + 2\arcsin k'\right)\sin\delta_s\end{aligned} \tag{23}$$

where k'= − sin(($\delta_{\min}-\delta_s$)/2). Substitute $\delta_{\max}$ and $\delta_{\min}$ back to k and k', the OF is

$$f(\delta_{\max},\delta_{\min}) = \frac{1}{T_u+T_r} = \frac{1}{\sum_{i=0}^{\infty}\left(t_{u,i}+t_{r,i}\right)} \tag{24}$$

An approximate OF formula can be obtained by keeping a finite number of terms in the denominator of (24), e.g. the formula (25) keeping only the first term.

$$f \approx \frac{\sqrt{\beta}}{\sqrt{2}\pi}\left(\frac{\sin\left((\delta_{\max}-\delta_s)/2\right)}{m(\delta_{\max})} + \frac{\sin\left((-\delta_{\min}-\delta_s)/2\right)}{m(\delta_{\min})}\right)^{-1} \tag{25}$$

$$m(x) = \sqrt{\cos\delta_s - \cos x - (\delta_s - x)\sin\delta_s} \tag{26}$$

The above power series based approach provides an analytic expression of the OF that summates an infinite series. Keeping finite terms can give a closed-form approximate OF for further analytical studies. In the rest of the paper, the OF is calculated numerically by the formulas in (6)-(8).

IV. Frequency-Amplitude Curve

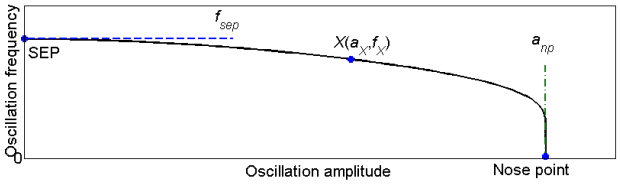

Fig.4. F-A curve of an undamped SMIB system

A. F-A curve

As illustrated in Fig.4, the F-A curve of an undamped SMIB power system is the characteristic of the OF with respect to the OA as defined by (8), where the OA can be either $\delta_{\max}-\delta_s$ or $|\delta_{\min}-\delta_s|$. The former one is used in the rest of the paper. The F-A curve is an exact characterization of the undamped oscillation of a disturbed SMIB system. It shows that the OF only depends on the OA when the system topology and operating condition are fixed. According to (6)-(8), two independent parameters β and δ_s are needed to determine the F-A curve. As shown in Fig.4, a point $X(a_X, f_X)$ on the curve indicates that the system is oscillating at frequency f_X with amplitude a_x. Thus, if one of the OF and OA is known, the other will be uniquely determined from the F-A curve. Some remarks are given:

1) Damping is ignored in the formulation

The conservation of energy law has been used in deriving the F-A curve for an undamped SMIB system. A general F-A curve for a damped SMIB system needs further investigation but is very close to the F-A curve of the corresponding undamped SMIB system as shown later in Section VI-A.

2) Only single-mode oscillation is considered

The formulation based on a SMIB system only considers a single EO mode. The exact formulation for one EO mode of a general multi-machine system is not a trivial effort, and will be in the future work. Without rigorous mathematic proof, this paper assumes that the F-A curve exists for each of EO modes (at least for each of dominant EO modes) of a multi-machine power system. In addition, this paper does not consider nonlinear modal interactions and only focuses on the nonlinearities inherent to each individual mode. All tests in this paper are designed to only exhibit the nonlinearities of one specific mode while behaviors of other modes are either nearly linear or not interacting with this mode due to distinct gaps between their OFs.

B. F-A curve based stability analysis

As a comparative concept, the P-V curve for voltage stability

analysis is a projection of the changing SEP until saddle-node bifurcation from a high-dimensional space onto a 2-D power-voltage plane. The proposed F-A curve is actually a projection of the trajectory of the system state from a high-dimensional space within the stability boundary onto a 2-D OF-OA plane, and therefore, it can be used for angle stability analysis.

As illustrated in Fig.4, the F-A curve intersects with OF and OA axes respectively at the SEP point $(0, f_n)$ and a "nose" point $(a_{np},0)$: at the SEP, the OA is zero and the OF equals the linear, natural frequency f_n; at the "nose" point, a_{np} gives the largest allowed OA for any stable oscillation, or in other words, a_{np} is actually the stability limit of the angle. These conclusions can be made: 1) the OF monotonically decreases with the increase of the OA; 2) when the OA gets closer to the limit, the OF drops more significantly.

It is pointed out that the "nose" point is the projection of part of the stability boundary which contains the controlling unstable equilibrium point (CUEP). Projected onto the 2-D OF-OA plane, an F-A curve can help visualize how the disturbed system state moves back to its SEP over time in a straightforward way. To this end, the phase diagram is adopted as a comparison in the introduction of the F-A curve based stability analysis.

A phase diagram about state variables is a powerful tool to show how the system state moves when disturbed. For a multi-machine system, when a large disturbance pushes the system to approach the CUEP, it is difficult to envision the system trajectory in a high-dimensional phase diagram having all state variables as axes, so a projection of the trajectory onto a 2-D or 3-D phase diagram about selected state variables is often used. Note that such a low-dimensional phase diagram can be interpreted only when proper axes, namely state variables, are chosen. For a power system with many generators, such proper axes may not easily be determined for each EO mode especially for an interarea mode. As a result, the resulting phase diagram may be obscure as illustrated by Fig.5 about a case on the IEEE 9-bus system studied later in section VI-B if two angle differences are selected as the axes.

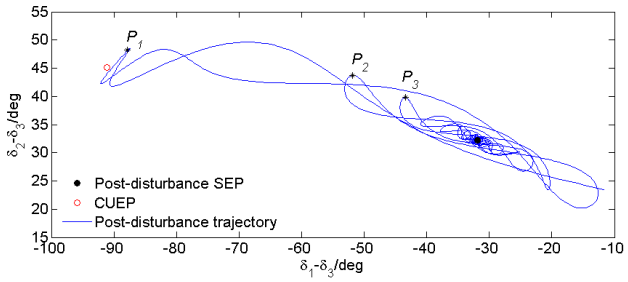

Fig.5. Post-disturbance phase trajectory of a marginally stable system

The proposed F-A curve based stability analysis projects the post-disturbance trajectory of the system state onto the 2-D OF-OA plane about a certain EO mode. In that plane, the disturbed system, if stable, will always monotonically move back to its SEP following an F-A curve. For instance, if the phase trajectory in Fig.5 is mapped to an F-A curve like Fig.4 about the dominant mode, point P_1 will be close to the "nose" point in Fig.4, and P_3 and the points thereafter will converge to the SEP. Thus, an F-A curve can directly visualize the trajectory of a stable multi-machine system onto a 2-D plane and clearly depict how the system returns to its SEP.

To analyze system stability under a given contingency, the F-A curve of the post-contingency system needs to be obtained first. Then, the largest OA or smallest OF from the measured system trajectories can be found on the F-A curve. Finally, the distance to the stability boundary can be defined as a stability margin index (SMI) of the system. The normalized SMI defined in (27) will be used for the rest of the paper to quantify the proximity to the "nose" point.

$$SMI = \left(1 - \frac{a_X}{a_{np}}\right) \times 100\% \tag{27}$$

C. F-A curve aided oscillation frequency estimation

For any EO with non-zero amplitudes, the observed OF is slightly smaller than f_n of this EO mode according to the F-A curve. Their difference is caused by the nonlinearity in oscillation such that any linear method will always give an OF estimate with some error. The upper bound of that OF error regarding one specific EO mode can be derived by means of the F-A curve. From (8), there are (28) and (29). For instance, given the F-A curve in Fig.4, the upper bound of the OF error is illustrated in Fig.6. For oscillations with small amplitudes, equation (25) can be utilized to obtain the OF and help calculate the upper bound in a fast way. This application of the F-A curve will not be the focus of the rest of the paper.

$$\left|e_f\right| \le f_n - \frac{1}{T_u + T_r} \tag{28}$$

$$f_n = \lim_{\delta_{max} \to \delta_s^+, \delta_{min} \to \delta_s^-} \frac{1}{T_u + T_r} = \frac{1}{2\pi}\sqrt{\beta \cos \delta_s} \tag{29}$$

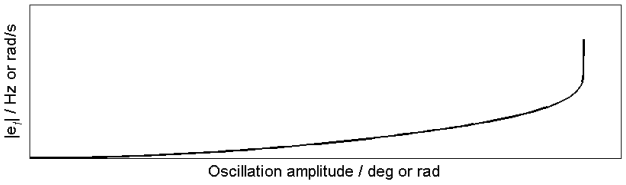

Fig.6. Upper bound of error of oscillation frequency estimation

V. Estimation of the F-A Curve from Measurements

The accurate estimation of the F-A curve from measurements is difficult because there is no general way for the construction of an ideal single-mode signal with respect to each oscillation mode by using only measurements, especially for large-amplitude oscillations with significant nonlinearities. However, an approximate F-A curve can be estimated directly by a measurement-based approach for a dominant EO mode under these two assumptions:

- *Assumption 1*: Other EO modes behave in a fairly linear manner, e.g. being not excited much to exhibit significant nonlinearities.
- *Assumption 2*: The F-A curve regarding a dominant EO mode of a multi-machine system is similar to the F-A curve of an equivalent SMIB system.

A. Measurement-based F-A curve estimation

A measurement-based approach for estimating an F-A curve about a specific dominant EO mode is proposed as shown in Fig.7, which first estimates a number of points on the F-A plane using a reconstructed single-mode signal from measurements, and then optimally estimates the F-A curve by solving an optimization problem.

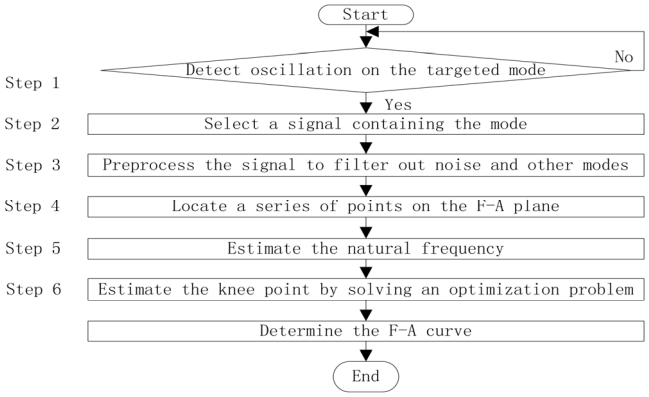

Fig.7. Flow chart of the F-A curve estimation.

1) Step-1: Signal selection

For a targeted dominant EO mode, identify two opposing groups of generators. If both groups have generators monitored by phasor measurement units (PMUs), the angle of the center of inertia (COI) $\delta_{COI,j}$ about those measured rotor angles in group J may represent the angle of the group:

$$\delta_{COI,j} = \sum_{i\in J} H_i\delta_i \Big/ \sum_{i\in J} H_i \tag{30}$$

Alternatively, the angle of a group may simply take one of measured rotor angles (note that if the rotor angle of a generator is not directly measured by the PMU, it may still be calculated from PMU data at other locations, e.g. by means of a dynamic state estimator [17][18]). Then the real-time angle difference between the two groups can be obtained as the input signal of the approach.

2) Step-2 Signal pre-processing

This step re-constructs a clean, single-mode oscillation signal, denoted by $\delta(t)$, from the input signal by filtering out noises and other oscillation modes.

3) Step-3: Locating a series of points on the OF-OA plane

Locate a series of points (a_1,f_1), (a_2,f_2), …, (a_N,f_N) on the F-A plane gradually approaching the SEP of the F-A curve:

i) Find the steady-state value (still denoted by δ_s) of signal δ by, e.g., the mean value of the signal over the last several swings when nonlinearity becomes negligible.

ii) Find extreme points on the signal to generate a series of points on the F-A curve as illustrated by Fig.8 and (31).

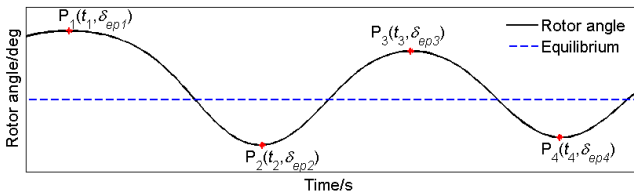

Fig.8. A typical single-mode oscillation signal

$$\begin{cases} a_1 = \left|\dfrac{\delta_{ep1}+\delta_{ep3}}{2} - \delta_s\right| \\ f_1 = \dfrac{1}{t_3 - t_1} \end{cases}, \qquad \begin{cases} a_2 = \left|\delta_{ep3} - \delta_{eps}\right|, \ldots \\ f_2 = \dfrac{1}{t_4 - t_2} \end{cases} \tag{31}$$

4) Step-4: Estimation of the natural frequency

The natural frequency f_n can be estimated using those estimated points in (31) close to the SEP. In this paper, the average of top 20% of estimated points in Step 3 having the smallest OAs is used to give an estimate of f_n, denoted by $\hat{f}_n$.

5) Step-5: Estimation of the nose point

This step is to estimate the OA a_{np} at the "nose" point, which is in the range between 0 and π. It can be obtained by solving the following optimization problem (32) finding an F-A curve $f^{a_{np},\hat{f}_n}(\bullet)$ of any SMIB system that have the minimum overall difference to estimated points (a_1,f_1), (a_2,f_2), …, (a_N,f_N) from Step 3. Each of those F-A curves $f^{a_{np},\hat{f}_n}(\bullet)$ only depends on the a_{np} to be solved and $\hat{f}_n$ based on (6)-(8) with the two equivalent parameters $\hat{\beta}$ and $\hat{\delta}_s$ determined by (33). Denote the estimated a_{np} by $\hat{a}_{np}$

$$\min_{a_{np}\in[0,\pi]} \sum_{i=1}^{N} \left(f_i - f^{a_{np},\hat{f}_n}(a_i)\right)^2 \tag{32}$$

$$\hat{\delta}_s = \frac{\pi - a_{np}}{2}, \quad \hat{\beta} = \frac{4\pi^2 \hat{f}_n^2}{\cos\hat{\delta}_s} \tag{33}$$

6) Step-6: Estimation of the F-A curve

Finally, with estimated parameters $\hat{f}_n$ and $\hat{a}_{np}$, the whole F-A curve is calculated using (6)-(8).

B. Discussions

Regarding the accuracy of the proposed approach, the measurement-based estimation of an F-A curve and the associated SMI is accurate when the aforementioned two assumptions are both satisfied; otherwise, errors will exist in the estimated F-A curve and SMI.

Besides, the shape of the F-A curve depends on what input signal is chosen to reconstruct a single-mode oscillation signal. From different input signals, the proposed estimation approach may generate different F-A curves even for the same EO mode. However, those F-A curves should have the same natural frequency, i.e. the same SEP, and similar shapes but different scales of the amplitude. That is very similar to the dependence of constructing a P-V curve from measurements in voltage stability analysis on where data are chosen. Also, the accuracy of an F-A curve depends on whether the concerned EO mode is dominant enough in the input signal.

Regarding the dominancy of the concerned EO mode, the estimation approach proposed in this paper has a better accuracy when the concerned mode has significant nonlinearities and is dominant among all EO modes in the input signal. If the concerned mode is the most dominant one, the oscillatory energy of the whole system can more easily excite nonlinear behaviors about the concerned mode. Thus, the estimated points in the OF-OA plane for solving the optimization problem (32) more spread out to lead to a more credible F-A curve. Therefore, the

dominancy of the concerned EO mode directly influences the accuracy of the estimated F-A curve.

The proposed approach is computationally efficient. In the next section, case studies are performed on an Inter Core™ i7-3770 3.4GHz desktop computer. The numerical calculation of a single F-A curve using (8) only takes about 0.08s. When F-A curves on multiple targeted EO modes are numerically calculated using the measurement-based estimation algorithm in Fig.7, it typically takes 1~2s in a MATLAB environment to compute and 90% of the time is used to solve the optimization problem in (32).

Since only two parameters, i.e. β and δ_s, are used to determine an F-A curve, a library of all possible F-A curves with different combinations of β and δ_s at a certain resolution can be generated offline and applied online to eliminate most of the online computational burdens.

VI. Case Studies

This section firstly investigates the damping effect on an F-A curve using a damped SMIB system and then illustrates the existence of the F-A curve for each of major EO modes in two multi-machine systems: the IEEE 9-bus system and a WECC 179-bus system. In the 9-bus system, a case study uses the concept of CUEP to show how the F-A curve based stability analysis works. For the 179-bus system, F-A curves are generated from different generator models (from the 2nd order classical model to detailed generator models with and without exciters) and the impact from the level of model details is studied. In simulations, all loads are modeled as constant impedances.

A. Test on the SMIB power system

The purpose of this test is to validate the measurement-based approach for estimating the F-A curve and investigate the impact from system damping. Use the SMIB system in Section II and let damping coefficient D range from 0.05 p.u. to 5 p.u., which basically covers all reasonable values. Then the simulated stable rotor angle trajectories under a contingency become damped oscillation curves. The F-A curve estimated from each simulated result is found approximately coinciding with the formulated one from the undamped SMIB. For example, when D=0.5 p.u. in Scenario 2 of Fig.3, the estimated F-A curve is shown in Fig.9. The proposed SMI of the system under this disturbance is 9.9%. Therefore, the proposed estimation approach also works on damped oscillations and the F-A curve is insensitive to the damping coefficient.

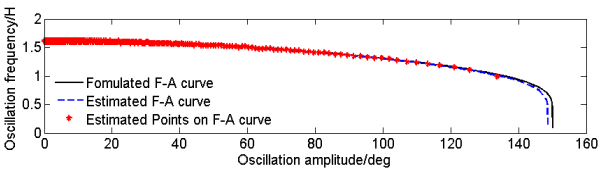

Fig.9. F-A curves from formulation and estimation

B. Test on the IEEE 9-bus system

This test is intent to show the existence of the F-A curve for each EO mode of a multi-machine system and to utilize the concept of CUEP to show how the proposed F-A curve based stability analysis method works. The tested IEEE 3-machine 9-bus system, as shown in Fig.10, represents all generators in the classical model and has two EO modes at 0.94Hz and 1.76Hz from small-signal analysis.

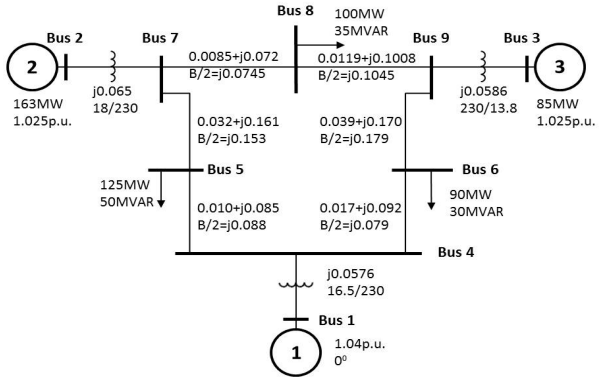

Fig.10. IEEE 9-bus system

1) Scenario 1: F-A curve of the 0.94Hz mode

In this scenario, a three-phase fault is added on bus 7 at t=1s and then cleared without tripping any line. The critical clearing time (CCT) identified by a number of simulation runs is 0.165s. Fig.11 shows the rotor angles with a fault clearing time of 0.16s, where the 0.94Hz mode is the dominant EO mode and the 1.76Hz is relatively quiescent. According to the small-signal analysis, generators 1 and 2 highly participate in the 0.94Hz mode and oscillate against each other. Thus, their angle difference is basically a single-mode oscillation signal and is selected as the input signal without preprocessing. The estimated F-A curve is shown in Fig.12 and the SMI under this disturbance is 34.4%.

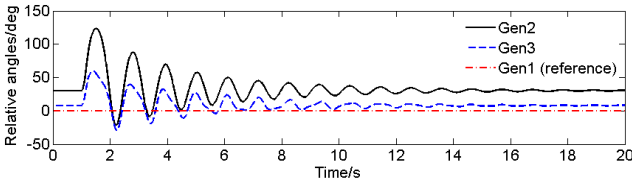

Fig.11. Relative angles in scenario 1.

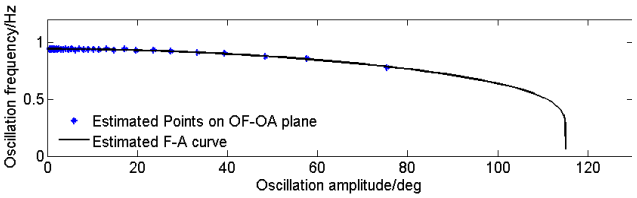

Fig.12. Estimated F-A curve for 0.94Hz mode in scenario 1.

2) Scenario 2: F-A curve of the 1.76Hz mode

To estimate the F-A curve for the 1.76Hz mode, this mode needs to be excited more than the 0.94Hz mode to become dominant. However, all three-phase bus faults in this system would always excite the 0.94Hz mode more, which means the system always loses its stability before exhibiting the nonlinear behavior of the 1.76Hz mode. To create a desired scenario, an excitation technique based on the concept of normal mode [20] is proposed to specifically excite a hidden mode for power system by initializing the system with linearly scaled mode shape of interest (for short, LSMS): the system is initialized with zero angular

velocities and the rotor angles are initialized at the linearly scaled mode shape about 1.76Hz. By doing this, the 1.76Hz mode is excited significantly while the 0.94Hz mode is not apparently excited. The relative rotor angles are shown in Fig.13. Modal analysis shows that generators 1 and 2 are oscillating together against generator 3 about the 1.76Hz mode. Hence, the angle difference between generator 3 and the COI of generators 1 and 2 is selected as the input signal. A high-pass filter (HPF) is applied to the signal and the resulting waveform is shown in Fig.14. FFT spectrums of waveforms before and after the filter are shown in Fig.15, which indicates that the signal after the HPF is basically a single-mode oscillation waveform. Fig.16 shows the estimated F-A curve with SMI=44.0%.

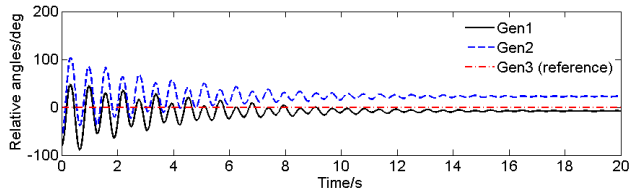

Fig.13. Relative angles in scenario 2

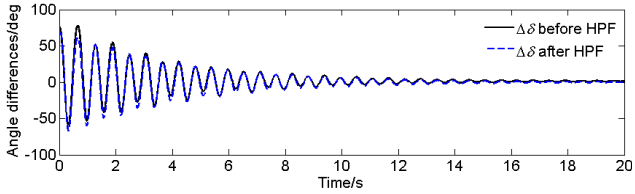

Fig.14. Angle differences before and after the HPF

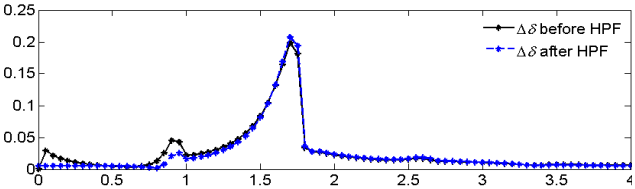

Fig.15. FFT spectrums before and after the HPF

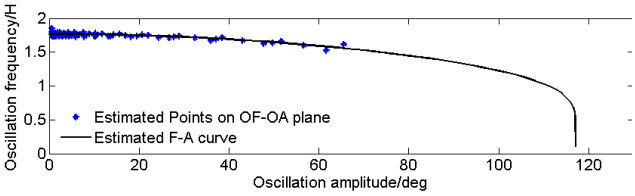

Fig.16. Estimated F-A curve for 1.76Hz mode in scenario 2

3) Scenario 3: F-A curve based stability analysis

A three-phase bus fault is added at bus 7 and cleared in a certain time by tripping the line 5-7. The CCT is found to be about 0.06s by a number of simulation runs. The small-signal analysis shows that two EO modes of the post-fault system have natural frequencies at 0.60Hz and 1.61Hz. If the fault is cleared at the CCT to create a marginally stable scenario, the post-fault rotor angles are shown in Fig.17 which indicates that the 0.60Hz mode is dominant. The angle difference between generators 1 and 2 is shown in Fig.18 as the input signal. A phase diagram about the input signal and its derivative is shown in Fig.19, where the CUEP is located using the BCU method [21]. The F-A curve estimated from the input signal is shown in Fig.20, where each point is calculated using data in one of oscillation periods (i.e. TW1, TW2, …) as shown in Fig.18. The F-A curve always tells how the system state moves from the stability boundary to the post-fault SEP. As a comparison, when selecting proper sub-space, e.g. the input signal for F-A curve, Fig.21 highlights the phase trajectory within each specified period, which expresses the same movements but in a different way. However, when selecting an improper sub-space, the phase diagram will be obscure as shown in Fig.5. The phase trajectories of the first four time windows are shown in Fig. 22 for comparison.

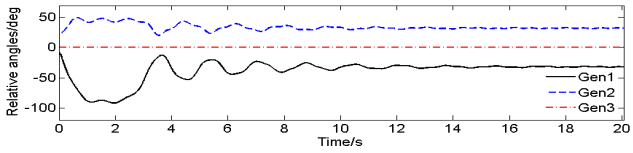

Fig.17. Relative angles in scenario 3.

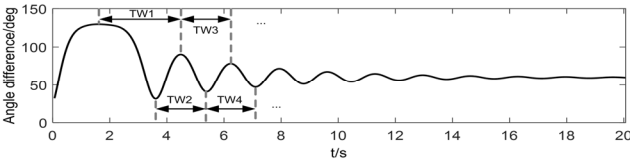

Fig.18. Angle difference between generators 1 and 2 in scenario 3.

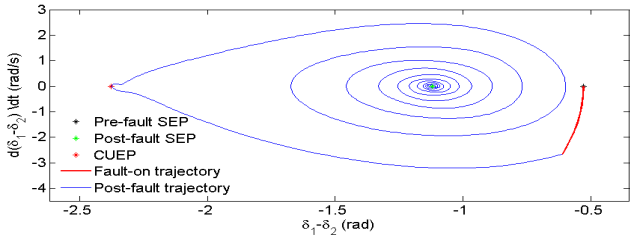

Fig.19. Phase trajectory of the system in scenario 3.

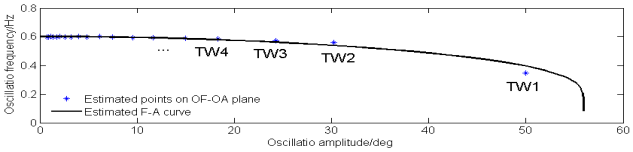

Fig.20. Estimated F-A curve for 0.6Hz mode in scenario 3.

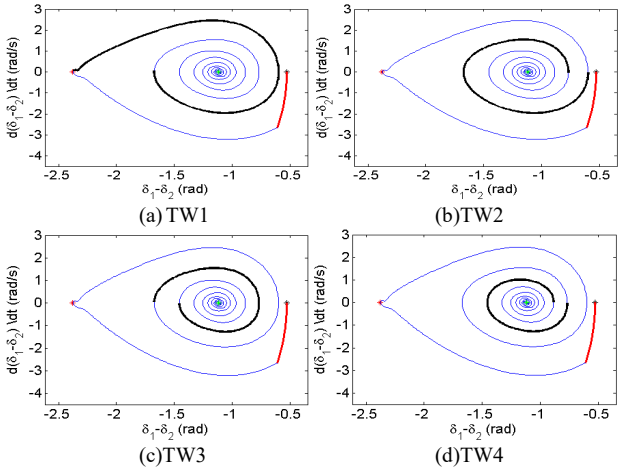

Fig.21. Phase trajectories of first four time windows

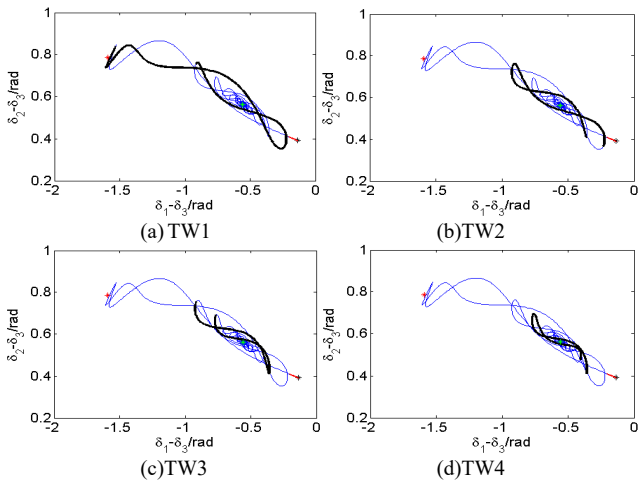

Fig.22. Phase trajectories of first four time windows in another phase subspace.

C. *Test on the WECC 179-bus system*

To study F-A curves of a large power system, the WECC 29-machine 179-bus system shown in Fig.23 is used. Small-signal analysis on the linearized system model suggests 28 EO modes.

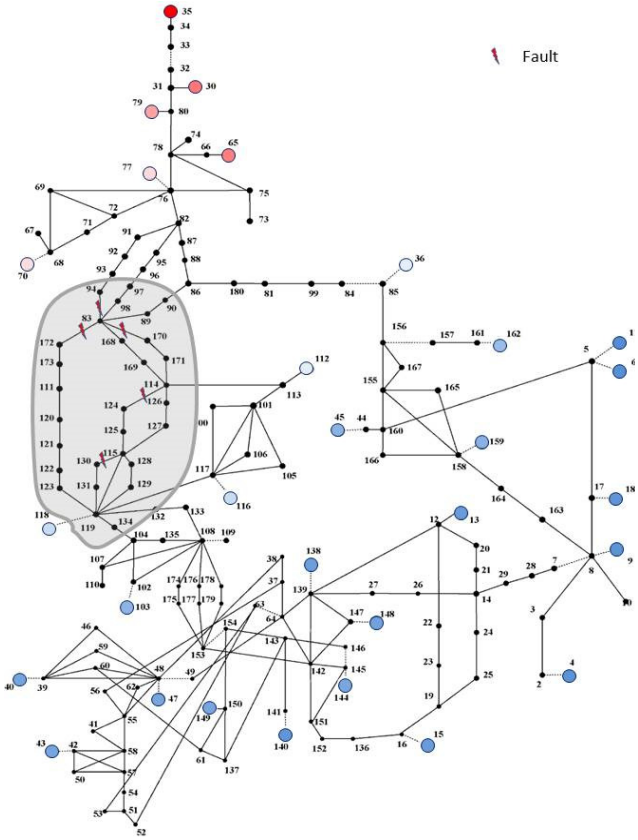

Fig.23. WECC 179-bus system

1) *Scenario 1: F-A curves on the dominant inter-area mode under cascading events*

The scenario is similar to the cascading events in [22] except that all generators are represented by the classical model and the damping is smaller such that EOs can be more observable following each event. Number this system model as *Model-1* to be distinguished from two more detailed system models numbered *Model-2* and *Model-3* considered later in Scenario 3. Consider five sequential three-phase faults on lines 83#-172, 83#-170, 114#-124, 115#-130 and 83#-94 at 40s intervals starting from *t*=0s, where "#" indicates the fault bus. These faults are designed to excite the well-known NS Mode A, which was involved in the Western North America blackouts on August 10, 1996 [23]. Small-signal analysis on the system model shows that this mode has a frequency at 0.28Hz and its mode shape is shown in Fig.23, where generators in red circles are oscillating against those in blue circles. How much each machine is involved is indicated by the darkness of the color. The angle difference between the COIs of the two groups is shown in Fig.24. Then, a low-pass filter (LPF) at 1.2Hz is then applied to weaken other modes. Finally, the estimated points on the F-A curve for each event and the estimated full F-A curve for the last event are shown in Fig.25. It can be seen that the OAs of the first four events are relatively small and their OFs roughly stay at their natural frequencies, respectively, while the OA of the last event reaches as large as 30° and its OF drops to around 0.17Hz whose SMI is about 30.9%. The frequency drop in the last event can also be observed in [22].

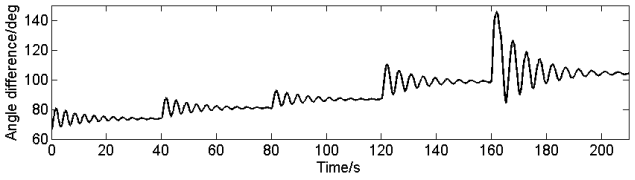

Fig.24. Angle difference of two groups of generators

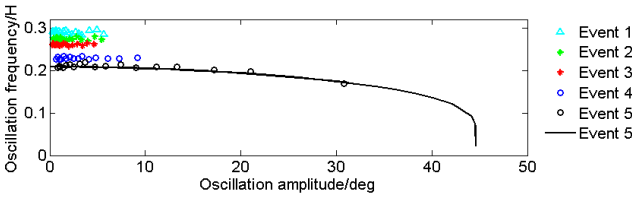

Fig.25. Estimated F-A curves for the 0.28Hz mode

2) *Scenario 2: F-A curves of other modes*

The second scenario shows the existence of the F-A curve for any other mode by using the LSMS excitation technique in Section VI-B. Fig.26 shows the estimated F-A curve for another inter-area mode at 0.44Hz, which is excited by setting the system initial conditions according to the LSMS excitation technique. From the F-A curve, the SMI of the system is about 64.5%. In addition, the F-A curves of some other selected modes are drawn in Fig.27, including three local modes above 1Hz. It can be seen that the F-A curve concept and associated estimation approach can apply to both local and inter-area EO modes.

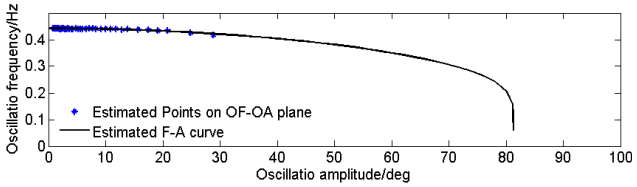

Fig.26. Estimated F-A curve for the 0.44Hz mode

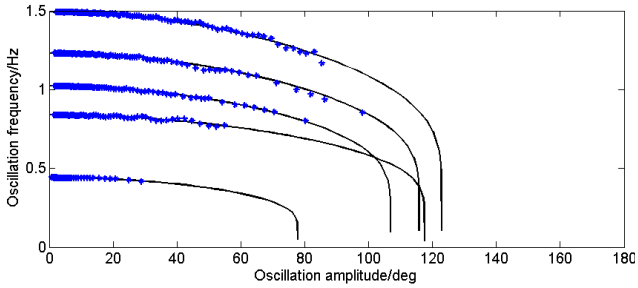

Fig.27. Selected F-A curves from system model-1

3) Scenario 3: F-A curves from systems in detailed models

By this scenario, the F-A curves of the system having generators represented in these two more detailed models are estimated and compared to the F-A curves from *Model-1*:

Model-2: all generators are in 4th-order model [24].

Model-3: all generators are in 4th-order model with exciters.

These two system models use the same power flow condition as *Model-1*. The SEXS exciter model in PSSE [25] is adopted for *Model-3* as shown in Fig.28. For simplicity, power system stabilizer and excitation limiters are not considered.

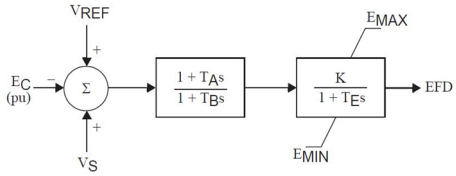

Fig.28. SEXS exciter model from PSSE model library

Some selected F-A curves from *Model-2* and *Model-3* are shown in Fig.29 and Fig.30, respectively. Comparing to the F-A curves in Fig.27, there is no significant difference for those modes except for the fastest mode with a natural frequency around 1.4Hz. It is not surprising because modes with lower OFs are associated with the oscillations between larger groups of generators and their interconnections in the power network. Therefore, the corresponding F-A curves are less sensitive to the level of details in generator models. In the contrary, the F-A curve corresponding to a local mode is related to individual generators in a local area and hence is more sensitive to the model details of those participating generators, especially the reactance used for connecting each generator to its terminal bus. Small signal analysis by Power System Toolbox [26] on *Model-2* and *Model-3* shows that the natural frequencies corresponding to the F-A curves in Fig.29 and Fig. 30 are almost the same as shown in Table III, since the natural frequencies are largely determined by the inertia constants of generators and network impedances which are actually the same for *model-2* and *model-3*. In addition, the comparison between Fig.29 and Fig.30 indicates that the added exciters do not significantly change the F-A characteristics of the multi-machine system.

TABLE III. SELECTED NATURAL FREQUENCIES IN *MODEL-2* AND *MODEL-3*

Modes	Selected natural frequencies in *Model-2*	Selected Natural frequencies in *Model-3*
0.4Hz mode	0.4425Hz	0.4316Hz
0.8Hz mode	0.8269Hz	0.8261Hz
1.0Hz mode	1.0236Hz	1.0194Hz
1.2Hz mode	1.1930Hz	1.1928Hz
1.4Hz mode	1.4144Hz	1.4141Hz

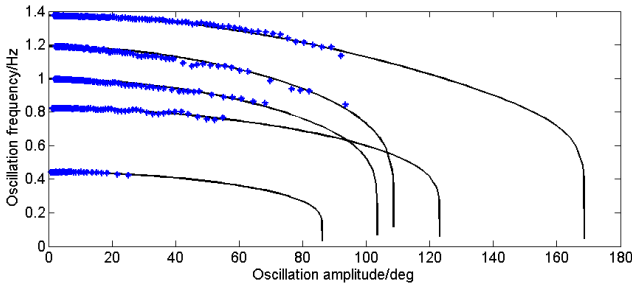

Fig.29. Selected F-A curves from system model-2

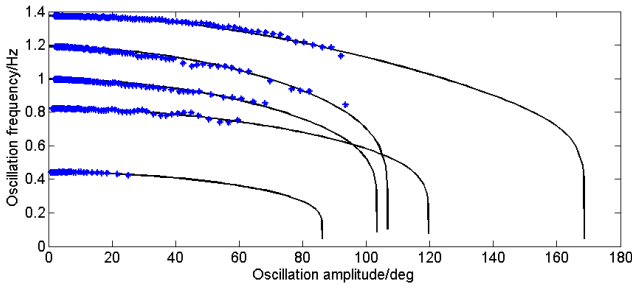

Fig.30. Selected F-A curves from system model-3

D. Discussions

1) Observation of F-A curves

The F-A curve is an intrinsic property of the EOs in power systems. However, it can be observed from measurements only when its associated mode is excited. How much of the curve can be observed largely depends on how significantly the mode is excited. Thus, if a mode is slightly excited, only a few points on its F-A curve can be observed around the SEP such as the first four events in Fig.25. When a certain mode is significantly excited while all other modes are only slightly excited, more points on the F-A curve could be observed by the proposed estimation approach such as the F-A curve in Fig.12 and the last event in Fig.25.

The LSMS excitation technique helps uncover some oscillatory behaviors of the system that may rarely occur under the most usual disturbances but are still credible and inherent with the system. With this excitation technique, any EO mode of a large system can be significantly excited while the other modes are relatively quiescent. However, if the initial condition determined by the LSMS excitation is too far from the nearly linear region around the SEP, other modes may also bring about their own nonlinearities into the resulting oscillations. In this case, nonlinear interactions between the concerned mode and other modes are no longer ignorable. Since the nonlinear modal interaction is not the focus of this paper, all tested scenarios involving LSMS excitation technique are carefully designed such that only the concerned mode is excited to exhibit nonlinearity while all other modes are almost linear. This is the reason why the

scenarios used for generating the F-A curves in Fig.27, Fig.29 and Fig.30 only contain parts of points on their F-A curves.

2) Intersection of F-A curves

Note that each F-A curve in Fig.27, Fig.29 and Fig.30 are generated from an independent LSMS excitation and represents the system's behavior following a specific disturbance. Therefore, even if the F-A curves of some different modes may intersect, they are from different disturbances and may not co-exist under the same condition.

VII. Conclusion

This paper introduces the nonlinearities of the power system electromechanical oscillations and formulates the oscillation frequency analytically on a SMIB power system. Based on the formulation, the F-A curve as a new nonlinear oscillation analysis and monitoring tool is proposed to characterize the energy-dependency of oscillations and used for angle stability analysis with respect to each oscillation mode. A measurement-based approach is proposed to estimate the whole F-A curve for any dominant oscillation mode in the measured post-disturbance system trajectories. The existence of the F-A curve for each oscillation mode is illustrated on the IEEE 9-bus system and the WECC 179-bus system.

Future research will include the analytical formulation of oscillation frequencies in multi-machine power systems considering nonlinear modal interaction, a general method for estimating the F-A curve from measurements and the application of the F-A curve based angle stability analysis.

References

[1] L. L. Grigsby, *The Electric Power Engineering Handbook*, Boca Raton: CRC Press, 2001

[2] G. Rogers, *Power System Oscillations*. New York: Springer, 2000

[3] A. R. Messina, *Inter-area Oscillations in Power Systems*. New York: Springer, 2009

[4] IEEE Task Force Report TP462, *Identification of Electromechanical Modes in Power Systems*, 2012

[5] A. R. Messina, *Wide-Area Monitoring of Interconnected Power Systems*. London: IET, 2015

[6] S. K. Starrett, A. A. Fouad, "Nonlinear measures of mode-machine participation," *IEEE Trans. Power Syst.*, Vol.13, no.2, pp.389-394, May 1998

[7] H. Amano, T. Kumano, T. Inoue, "Nonlinear stability indexes of power swing oscillation using normal form analysis," *IEEE Trans. Power Syst.*, Vol.21, no.2, pp.825-834, May 2006

[8] J. F. Hauer, C. J. Demeure, L. L. Scharf, "Initial results in Prony analysis of power system response signals," *IEEE Trans. Power Syst.*, Vol.5, no.1, pp.80-89, Feb. 1990

[9] J. N. Juang, R. S. Pappa, "An eigensystem realization algorithm for modal parameter identification and model reducton," *J. of Guidance, Control, and Dynamics*, Vol.8, no.5, pp.620-627, Sep. 1985

[10] Y. Hua, T. K. Sarkar, "Matrix pencil method for estimating parameters of exponentially damped/undamped sinusoids in noise," *IEEE Trans. Acoustic Speech*, Vol.38, no.5, pp.814-824, May 1990

[11] N. E. Huang, Z. Shen, S. R. Long, M. C. Wu, H. H. Shih, Q. Zheng, N. C. Yen, C. C. Tung, H. H. Liu, "The empirical mode decomposition and the Hilbert spectrum for nonlinear and non-stationary time series analysis," *Proc. R. Soc. Lond. A*, Vol.454, no., pp.903-995, 1998

[12] P. Maragos, J. Kaiser, T. Quatieri, "On amplitude and frequency demodulation using energy operators," *IEEE Trans. Signal Process.*, Vol.41, no.4, pp.1532-1550, Apr. 1993

[13] B. Wang, K. Sun, A. D. Rosso, E. Farantatos, N. Bhatt, "A study on fluctuations in electromechanical oscillation frequencies of power systems," *IEEE PES General Meeting*, National Harbor, MD, Jul. 2014

[14] B. Trento, B. Wang, K. Sun, L.M. Tolbert, "Integration of phase-locked loop based real-time oscillation tracking in grid synchronized systems," *IEEE PES General Meeting*, National Harbor, MD, Jul. 2014

[15] N. Duan, B. Wang, K. Sun, J. Ning, "Analysis of power system oscillation frequency using differential Groebner basis and the harmonic balance method," *IEEE PES General Meeting*, Denver, CO, Jul. 2015

[16] Y. Zhao, Y. Zhang, L. Chen, Y. Min, "Study on nonlinearity in power system Electromechanical oscillation," *Power System Technology*, Vol.36, no.10, pp.172-177, Oct. 2012

[17] N. Zhou, D. Meng, S. Lu, "Estimation of the dynamic states of synchronous machines using an extended particle filter," *IEEE Trans. Power Syst.*,vol.28, no.4, pp.4152-4161, Nov. 2013

[18] J. Qi, K. Sun, W. Kang, "Optimal PMU placement for power system dynamic state estimation by using empirical observability Gramian," *IEEE Trans. Power Syst.*,vol.30, no.4, pp.2041-2054, Jul. 2015

[19] B. Wang, K. Sun, X. Su, "A decoupling based direct method for power system transient stability analysis," *IEEE PES General Meeting*, Denver, CO, Jul. 2015

[20] R.E. Blake, "Basic Vibration Theory," *Shock and Vibration Handbook*, New York: McGraw Hill, 1988

[21] H.D. Chiang, F. Wu, P. Varaiya, "A BCU method for direct analysis of power system transient stability," *IEEE Trans. Power Syst.*, vol.9, no.3, pp.1194-1208, Aug 1994

[22] K. Sun, Q. Zhou, Y. Liu, "A phase locked loop-based approach to real-time modal analysis on synchrophasor measurement," *IEEE Trans. Smart Grid*, Vol.5, no.1, pp.260-269, Jan. 2014

[23] D. N. Kosterev, C.W. Taylor, W.A. Mittelstadt, "Model validation for the August 10, 1996 WSCC system outage," *IEEE Trans. Power Syst.*,vol.14, no.3, pp.967-979, Aug 1999

[24] B. Wang, K. Sun, "Power System Differential-Algebraic Equations," *arXiv:1512.05185*, Dec. 2015

[25] Siemens Power Technologies International, "PSS/E Model Library," PSSE/33.1.1, May 2012

[26] J.H. Chow and K.W. Cheung, "A toolbox for power system dynamics and control engineering education and research," *IEEE Trans. Power Syst.*, vol.7, no.4, pp.1559-1564, Nov 1992